Exosomal B7–H4 from irradiated glioblastoma cells contributes to increase FoxP3 expression of differentiating Th1 cells and promotes tumor growth

Yunhong Tian [a,b,1], Chunshan Liu [a,b,1], Zhiyong Li [c,1], Meiling Ai [a,b,1], Baiyao Wang [a,b], Kunpeng Du [a,b], Wei Liu [a,b], Hongmei Wang [a,b], Peng Yu [a,b], Chengcong Chen [a,b], Jie Lin [a,b], Anan Xu [a,b], Rong Li [a,b], Weijun Zhang [a,b,*], Yawei Yuan [a,b,**]

[a] *Department of Radiation Oncology, Affiliated Cancer Hospital & Institute of Guangzhou Medical University, Guangzhou, Guangdong Province, People's Republic of China*
[b] *State Key Laboratory of Respiratory Disease, Affiliated Cancer Hospital & Institute of Guangzhou Medical University, Guangzhou, People's Republic of China*
[c] *Department of Neurosurgery, Nanfang Hospital, Southern Medical University, Guangzhou, Guangdong Province, People's Republic of China*

ARTICLE INFO

ABSTRACT

Background: Glioblastoma (GBM) is the most common and aggressive form of primary brain tumor. Although numerous postoperative therapeutic strategies have already been developed, including radiotherapy, tumors inevitably recur after several years of treatment. The coinhibitory molecule B7–H4 negatively regulates T cell immune responses and promotes immune escape. Exosomes mediate intercellular communication and initiate immune evasion in the tumor microenvironment (TME).
Objective: This study aimed to determine whether B7–H4 is upregulated by radiation and loaded into exosomes, thus contributing to immunosuppression and enhancing tumor growth.
Methods: Iodixanol density-gradient centrifugation and flow cytometry were used to verify exosomal B7–H4. Naïve T cells were differentiated into Th1 cells, with or without exosomes. T cell-secreted cytokines and markers of T cell subsets were measured. Mechanistically, the roles of B7–H4, and ALIX in GBM were analyzed using databases and tissue samples. Co-immunoprecipitation, and pull-down assays were used to tested the direct interactions between ATM and ALIX or STAT3. *In vitro* ATM kinase assays, western blotting, and site-directed mutation were used to assess ATM-mediated STAT3 phosphorylation. Finally, the contribution of exosomal B7–H4 to immunosuppression and tumor growth was investigated *in vivo*.
Results: Exosomes from irradiated GBM cells decreased the anti-tumor immune response of T cell *in vitro* and *in vivo* via delivered B7–H4. Mechanistically, irradiation promoted exosome biogenesis by increasing the ATM-ALIX interaction. Furthermore, the ATM-phosphorylated STAT3 was found to directly binds to the *B7–H4* promoter to increase its expression. Finally, the radiation-induced increase in exosomal B7–H4 induced FoxP3 expression during Th1 cell differentiation via the activated STAT1 pathway. *In vivo*, exosomal B7–H4 decreased the radiation sensitivity of GBM cells, and reduced the survival of GBM mice model.
Conclusion: This study showed that radiation-enhanced exosomal B7–H4 promoted immunosuppression and tumor growth, hence defining a direct link between irradiation and anti-tumor immune responses. Our results suggest that co-administration of radiotherapy with anti-B7–H4 therapy could improve local tumor control and identify exosomal B7–H4 as a potential tumor biomarker.

---

* Corresponding author. Department of Radiation Oncology, Affiliated Cancer Hospital & Institute of Guangzhou Medical University, Guangzhou, Guangdong Province, People's Republic of China.
** Corresponding author. Department of Radiation Oncology, Affiliated Cancer Hospital & Institute of Guangzhou Medical University, Guangzhou, Guangdong Province, People's Republic of China.
E-mail addresses: 680335195@qq.com (W. Zhang), yuanyawei@gzhmu.edu.cn (Y. Yuan).
[1] Contributed equally.

1. Background

Glioblastoma (GBM) is an incurable and fatal tumor among adults, which originates from the central nervous system (CNS). GBM is the most common primary malignant brain tumor with an incidence rate of 3.20 per 100,000 population in the USA [1]. Current standard treatment for newly diagnosed GBM comprises surgical resection, adjuvant radiotherapy, and temozolomide chemotherapy [2]. Despite these aggressive strategies, radio-resistance leads to tumor recurrence in most patients and results in a median overall survival (OS) of only 12–15 months after diagnosis [2,3]. Thus, it is imperative to investigate the underlying mechanism of tumor recurrence after irradiation to improve patient prognosis.

Components within the tumor microenvironment (TME) have pivotal roles in determining radiotherapy outcomes [4,5]. In GBM, the TME is infiltrated with leukocytes, mostly T helper (Th) cells, and $CD4^+CD25^+FoxP3^+$ regulatory T (Treg) cells. It has been found that effector $CD4^+$ Th1 cells promote tumor destruction, while Treg cells are associated with poor prognosis in GBM through their inhibition of the antitumor responses [6,7]. Moreover, radiation has been shown to have immunological effects, including the occasional induction of systemic antitumor response, the so-called "abscopal effect", and enhanced immunosuppression [8]. However, the relationship between irradiated GBM and tumor-infiltrating T cells is undetermined.

The B7–H4 (v-set domain containing T cell activation inhibitor 1, VTCN1, also known as B7x), expressed on various tumor cells, is a member of the CD28/B7 family of immune co-inhibitory molecules. B7–H4 activity is associated with a decreased inflammatory $CD4^+$ T cell response and increased Tregs within the TME [9]. Meanwhile, programmed death-ligand 1 (PD-L1), another co-inhibitory molecule, is found on the surface of exosomes [10]. Exosomes comprise a heterogeneous group of cell-derived membranous structures of ~40–160 nm in diameter [11]. Exosomes are involved in GBM tumor progression and TME modification, and are thus emerging as potential therapeutic targets of tumors [12,13]. Whether exosomal B7–H4, which might induce local immunosuppression, can be detected in irradiated GBM cells is unknown.

Therefore, the present study investigated the role of irradiation in GBM cells secreting exosomal B7–H4 and in the T cell immune response. Exosomes from irradiated GBM cells were observed to inhibit the antitumor immune potential of T cells and promote tumor growth. Furthermore, irradiation promoted exosome production by increasing the interaction between the kinase ataxia telangiectasia mutated (ATM) and apoptosis-linked gene 2-interacting protein X (PDCDIP, also known as ALIX) and induced B7–H4 expression via ATM-mediated phosphorylation of signal transducer and activator of transcription 3 (STAT3). Finally, exosomal B7–H4 enhanced Foxp3 expression of differentiating Th1 cells via STAT1 pathway inactivation.

2. Materials and methods

2.1. Cell lines and culture

Murine GL261, human GBM cells LN229 and LN308, and human embryonic kidney (HEK) 293T cells were purchased from the cell bank of the Chinese Academy of Sciences (Shanghai, China). All cells were cultured in Dulbecco's Modified Eagle Medium (DMEM) with 1% sodium pyruvate and 1% nonessential amino acids (Gibco, Gaithersburg, MD, USA), containing 10% fetal bovine serum (FBS, Gibco), and 1% penicillin-streptomycin (Gibco). All cells tested negative for mycoplasma contamination.

2.2. Patient and tumor samples

Paraffin-embedded tissue samples from 166 GBM patients from two hospitals, including Nanfang Hospital of Southern Medical University (Guangzhou, Guangdong, China), and Affiliated Cancer Hospital & Institute of Guangzhou Medical University (Guangzhou), were obtained from January 2016 to January 2019. All patients had received adjuvant radiotherapy and temozolomide chemotherapy after surgery. All samples were collected after the patients provided their signed informed consent according to the internal review and ethics boards of these hospitals. The GBM diagnosis was confirmed by histopathology.

2.3. T Cell isolation and differentiation

Peripheral blood mononuclear cells (PBMCs) were isolated from healthy donor blood samples using the Ficoll density gradient separation (GE Healthcare, Chicago, IL, USA) according to the manufacturer's protocols. A portion of the PBMCs was subjected to T cell separation using anti-human CD3 beads (STEMCELL Technologies, Vancouver, Canada); isolated cells were measured using flow cytometry. To differentiate human naïve $CD4^+$ T cells into Th1 cells, naive $CD4^+$ T cells were separated using an EasySep human naïve $CD4^+$ T cell isolation kit (STEMCELL Technologies) to negatively select for $CD4^+CD45RO^-$ cells from PBMCs according to the manufacturer's protocols. The naïve $CD4^+$ T cells were stimulated with human CD3/CD28 T cell activator (STEMCELL Technologies) and human Th1 differentiation supplement (STEMCELL Technologies), and were cultured in Roswell Park Memorial Institute (RPMI) 1640 medium. On day 3, differentiated Th1 cells are ready for use.

2.4. Exosome purification and preparation of cell lysates

Cells were grown to 80% confluency, rinsed with phosphate-buffered saline (PBS) and refreshed with DMEM supplemented with 10% exosome-depleted FBS (Gibco). The cell-conditioned medium (CM) was collected 48 h later, pooling the media from triplicate cultures. Exosomes were purified from the CM using differential centrifugation [14]. Briefly, CM was subjected to sequential centrifugation at 300, 2000, and $10,000 \times g$ before pelleting the exosomes at $100,000 \times g$ in a SW41Ti swinging bucket rotor for 3 h (Beckman Coulter, Brea, CA, USA). The exosomal pellets were resuspended in PBS or lysis buffer (PBS with 1% NP40, 1 mM EDTA, 5 μg/mL leupeptin, 1 μg/mL pepstatin, and 1 mM phenylmethylsulphonyl fluoride). A bicinchoninic acid (BCA) protein assay kit (Pierce, Rockford, IL, USA) was used to measure the exosomal protein content. The corresponding cell layers were washed twice with cold PBS, and were scraped on ice with the lysis buffer. The cell lysates from triplicate cultures were pooled, and cleared by centrifugation at 12,000×g, for 15 min at 4 °C. The cell lysates were normalized by their protein content.

2.5. Characterization of the purified exosomes

Nanoparticle tracking analysis (NTA) was used to determine the size and number of the purified exosomes. Briefly, background measurements were performed with filtered PBS, which revealed the absence of any kinds of particles. Exosomes diluted 1:1000 with PBS were analyzed using a Nanosight NS300 instrument with the NTA 3.0 software (Malvern Instruments, Malvern, UK) for five repeated analyses. For iodixanol density-gradient centrifugation, exosomes were loaded on top of a discontinuous iodixanol gradient (5%, 10%, 20%, and 40%) and ultracentrifuged at $100,000 \times g$ for 18 h at 4 °C (Beckman Coulter). Twelve equal volume fractions were collected from the top of the gradients, with the exosomes were found to be distributed at a density between 1.13 and 1.19 g/mL, as previously demonstrated [10]. The exosomes were further pelleted by ultracentrifugation at $100,000 \times g$ for 2 h at 4 °C.

2.6. Coincubation of T cells with exosomes or GBM cells

Exosomes were added to naïve T cells cultured in RPMI 1640 medium with the human CD3/CD28 T cell activator and Th1 differentiation

supplement. T cells for other assays were cultured for 72 h and harvested. To assay the proliferation of T cells, carboxyfluorescein diacetate succinimidyl ester (CFSE) (Thermo Fisher Scientific, Waltham, MA) was used to track cell division. Briefly, T cells (1×10^6/well) were incubated with 5 μM of CFSE at 37 °C for 20 min and the reaction was stopped by adding 5 vol of cold medium with 10% FBS, and treated. Unstimulated CFSE-labeled cells served as a nondividing control. For GBM cells cocultured with T cells, confluent microwell cultures of GBM cells were washed and activated T cells (5×10^4) were added to the medium. T cells or their supernatants were harvested 48 h after coculture with GBM cells.

2.7. In vitro ATM kinase assay

The *in vitro* ATM kinase assay was performed as previously described [15]. Briefly, myc-tagged ATM was immunoprecipitated (IP) from transiently transfected HEK293T cells, with or without irradiation at 4 Gy. The ATM-IP product was washed three times with IP buffer followed by 1 X kinase buffer (10 mM HEPES pH 7.5, 50 mM glycerophosphate, 50 mM NaCl, 10 mM $MgCl_2$, 10 mM $MnCl_2$, 5 μM ATP, and 1 mM dithiothreitol). Recombinant STAT3 (100 ng; Abcam) was incubated with 15 μL of ATM-IP, and 2.5 μCi of γ-32P-ATP (Perkin Elmer, Waltham, MA, USA) at 30 °C for 30 min. The reaction was terminated by adding SDS sample buffer, heated at 95 °C for 5 min, and then subjected to SDS-PAGE and autoradiography.

2.8. Cytokine array and enzyme linked immunosorbent assay (ELISA) analysis of inflammatory cytokines

Activated T cells were co-cultured with GBM-derived exosomes, with or without irradiation, for 48 h. The supernatant was exosome-depleted and was applied to a Proteome Profiler™ Human Cytokine Array Kit (ARY005B, R&D Systems, Minneapolis, MN, USA). The spot intensity was quantified using the Protein Array Analyzer ImageJ Plugin and normalized to the cell count as previously described [16]. The harvested CM was further analyzed for IFN-γ, tumor necrosis factor alpha (TNF-α), and interleukin 1 receptor antagonist (IL-1ra) using an ELISA Kit (R&D Systems) according to the manufacturer's protocols.

2.9. Plasmid transfection

GBM or HEK293T cells were transfected with plasmids using Lipofectamine 3000 (Invitrogen, Carlsbad, CA, USA), according to the manufacturer's instructions. Transfection efficiency was verified by western blotting. Naïve $CD4^+$ T cells were transfected with plasmids using the Human T Cell Nucleofector Kit and Amaxa Nucleofector system (Lonza, Cologne, Germany) as described in the manufacturer's protocol. Briefly, naïve $CD4^+$ T cells were harvested and resuspended in 100 μL of human T cell nucleofector solution, and 10 μg plasmid was added. Cells were electroporated using the nucleofector program V-024 in the Amaxa Nucleofector apparatus (Lonza) and were cultured in RPMI 1640 complete medium (Gibco), which was replenished 6 h after transfection. The cells were harvested for subsequent experiments.

2.10. In vivo murine studies

All experiments were carried out according to the United States Public Health Service (USPHS) guide for the care and use of laboratory animals and the China animal welfare regulations, and were approved by the animal care committee of Guangzhou Medical University (Guangzhou). For tumor challenge and adoptive transfer, female NOD/SCID mice (4–6 weeks old) were injected subcutaneously (s.c.) into each hind limb with 5×10^5 cells in 100 μL of DMEM. Two weeks later, the mice whose tumor volumes reached approximately 100 mm^3 were treated with or without radiation, with a total dose of 10 Gy on days 15 and 16. For adoptive transfer, cells harvested from spleens were

enriched for $CD45.2^+CD3^+$ T cells using an EasySep™ Mouse T Cell Isolation Kit (STEMCELL Technologies) and labeled with 2 μM CFSE. Forty-eight h after the last irradiation, the tumor-bearing mice were injected intravenously with 5×10^6 CFSE-labeled *in vitro* activated T cells. Five days later, the cell counts of adoptively transferred T cells in the blood and that had infiltrated the spleen and tumors were determined using flow cytometry. To establish a GBM model in C57BL/6 mice or NOD/SCID mice, GL261 cells or GL261 cells with a *B7–H4* short hairpin RNA (shRNA) (5×10^5 cells in 100 μL medium) were injected s. c. into mice. Two weeks later, the tumors were irradiated. In addition, 200 μL of 0.3 mg/mL GW4869 (Sigma-Aldrich, St. Louis, MO, USA) in 0.9% normal saline (2–2.5 μg/g body weight) or 200 μL of 3.75% DMSO saline control were injected intraperitoneally every 48 h from day 15. Mice were sacrificed 24 h after the final injection. To investigate the OS of the constructed mice models, the mice were implanted intracranially with GL261 cells. A total of 3×10^5 cells in 5 μL of PBS were injected using a Hamilton syringe 1 mm caudal to the central suture and 2 mm lateral to the bregma, at a depth of 3 mm. Then, the mice were treated with radiation and GW4869 following the same protocol described above. Survival endpoints were recorded and analyzed.

2.11. Western blotting

Cells and exosomes were lysed using Radio Immunoprecipitation Assay Lysis (RIPA) buffer containing a protease inhibitor cocktail (Sigma). The lysed samples were centrifuged at $12,000 \times g$ for 15 min at 4 °C, and the supernatant was collected. Protein concentrations were measured using the BCA protein assay. Protein samples in 3 X loading buffer (Thermo Fisher Scientific) were boiled for 5 min at 90 °C. Lysates (20–30 μg) were subjected to SDS polyacrylamide gel electrophoresis (SDS-PAGE) and the separated proteins were the transferred electrophoretically onto polyvinylidene fluoride membranes. The membranes were blocked in bovine serum albumin at room temperature for 1 h and were then incubated with primary antibodies at 4 °C overnight. After washing and incubating with the appropriate horseradish peroxidase-conjugated secondary antibodies, the immunoreactive protein bands were visualized using Imager (Bio-Rad Laboratories, Hercules, CA, USA) with the ECL western blotting substrate (Pierce). Western blotting experiments were repeated three times independently with similar results.

2.12. Immunohistochemistry (IHC)

IHC was performed on 4 μm-thick tissue sections prepared from the paraffin-embedded tissue blocks. The tissue sections were fixed in 4% formalin for 24 h before paraffin embedding. After deparaffinization and hydration, the sections were then pre-treated with sodium citrate buffer in a microwave for antigen retrieval and blocked using normal goat serum. The sections were incubated with antibodies for B7-H4, ALIX, and STAT3 (all Abcam, Cambridge, MA, USA) overnight at 4 °C, and then were incubated with biotinylated goat anti-rabbit IgG secondary antibodies for 1 h. Finally, the sections were stained using an avidin-biotin peroxidase complex (GeneTex, Irvine, CA, USA). Two independent pathologists performed the section scoring.

2.13. Profiling of genes co-expressed with ATM

LinkedOmics (http://www.linkedomics.org/login.php) is a publicly available database for online analysis of multi-omics data across 32 cancer types from The Cancer Genome Atlas (TCGA) database [17]. In LinkedOmics, genes that were co-expressed with ATM were identified using Pearson's correlation analysis. The association results were displayed as heat maps. Kyoto Encyclopedia of Genes and Genomes (KEGG) pathway analysis and gene set enrichment analysis (GSEA) were performed for the functional annotation of the ATM-related genes. Other published glioma transcriptome datasets were downloaded from the Chinese Glioma Genome Atlas (CGGA). The RNA sequencing data were
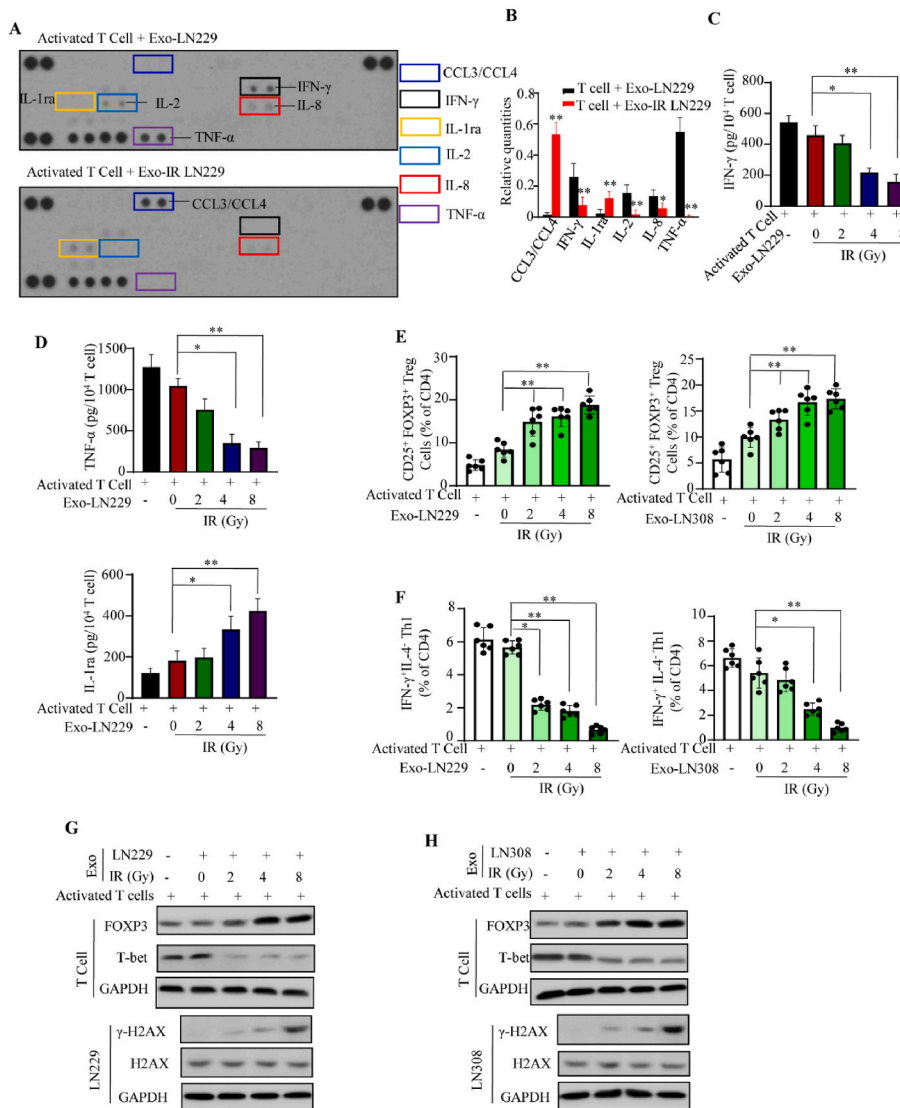
Fig. 1. Irradiated glioblastoma (GBM) cells contributes to immunosuppression *in vitro*. (**A–D**) Effect of exosomes from irradiated LN229 cells on inflammatory cytokines secreted by T cells. (**A**) Cytokine array analysis of systemic inflammatory cytokines secreted by exosome-treated T cells. (**B**) Quantitative summary of the cytokine array analysis in (**A**) (n = 3). (**C–D**) Quantitative summary of the concentrations of IFN-γ (**C**), TNF-α, and IL-1ra (**D**) in the media as detected using ELISA (n = 4). (**E–F**) Frequency of diverse subsets within T cells treated using exosomes from GBM cells, with or without irradiation (n = 6). (**G–H**) T cells treated using exosomes from GBM cells, with or without irradiation, were harvested. The protein levels of T-bet and Foxp3 were determined using western blotting. (IR: irradiation; Exo: exosomes. *P < 0.05, **P < 0.01 *vs.* the control.)

log2 transformed before doing an analysis between different groups. Differentially expressed genes (DEGs) between different groups were identified with the criteria of |fold change| >2 and a false discovery rate (FDR) < 0.05.

2.14. Flow cytometry

T cells were washed with PBS containing 0.1% FBS and stained using antibodies for CD3, CD4, CD8, CD25, CD44, CD62L, interleukin (IL)-4, IFN-γ, FoxP3, PD-1, Tim-3 and granzyme antibodies (all from BD Biosciences, San Jose, CA, USA). To assess cell death, T cells were stained for active caspase-3 according to manufacturer's instructions (Thermo Fisher Scientific). Cell proliferation was measured using CFSE staining. For intracellular flow cytometry, a fixation and permeabilization buffer was utilized (BD Biosciences). Cell surface staining was performed for 30 min at 4 °C. Meanwhile, intracellular staining was performed for 60 min on ice after using a fixation/permeabilization kit (BD Biosciences). Finally, flow cytometry was performed on a FACS LSR II or Fortessa instrument (BD Biosciences) and the data were analyzed using FlowJo 7.6 software (TreeStar, Ashland, OR, USA). Live or dead cells were discriminated using a Live/Dead Fixable Aqua Dead Cell Stain Kit (Thermo Fisher Scientific). Cell surface and intracellular staining were performed according to the manufacturer's instructions.

2.15. Co-immunoprecipitation (Co-IP) assay

Cell lysates (200–400 μg) were prepared in IP buffer and incubated with Protein A/G beads (GE Healthcare) at 4 °C for 1 h with gentle rotation. After centrifugation at 500×g for 1 min, the precleared lysates were incubated with the appropriate antibody at 4 °C for 12 h with gentle rotation. The Protein-A/G beads were added and incubated for another 3 h. Immunoprecipitates were collected by centrifugation at 500×g for 1 min, washed three times with IP buffer, and then heated at 95 °C for 5 min in 20 μL loading buffer for SDS-PAGE.

2.16. Chromatin immunoprecipitation (ChIP) assay

ChIP assays were performed using a Pierce Agarose ChIP Kit (Thermo Fisher Scientific) following the manufacturer's protocol. Briefly, cells were cultured to reach a confluency about 1×10^7 and cross-linked using 1% formaldehyde. Cell samples were harvested and resuspended in IP buffer supplemented with a protease inhibitor cocktail (Sigma). Then, cell suspensions were subjected to ultrasonication to break the nuclear membrane and shear the genomic DNA into 150–900 bp fragments. The final lysates were immunoprecipitated using either control IgG or STAT3 primary antibodies (Invitrogen). After washing and reversing the cross-links, the eluted DNAs fragments were evaluated
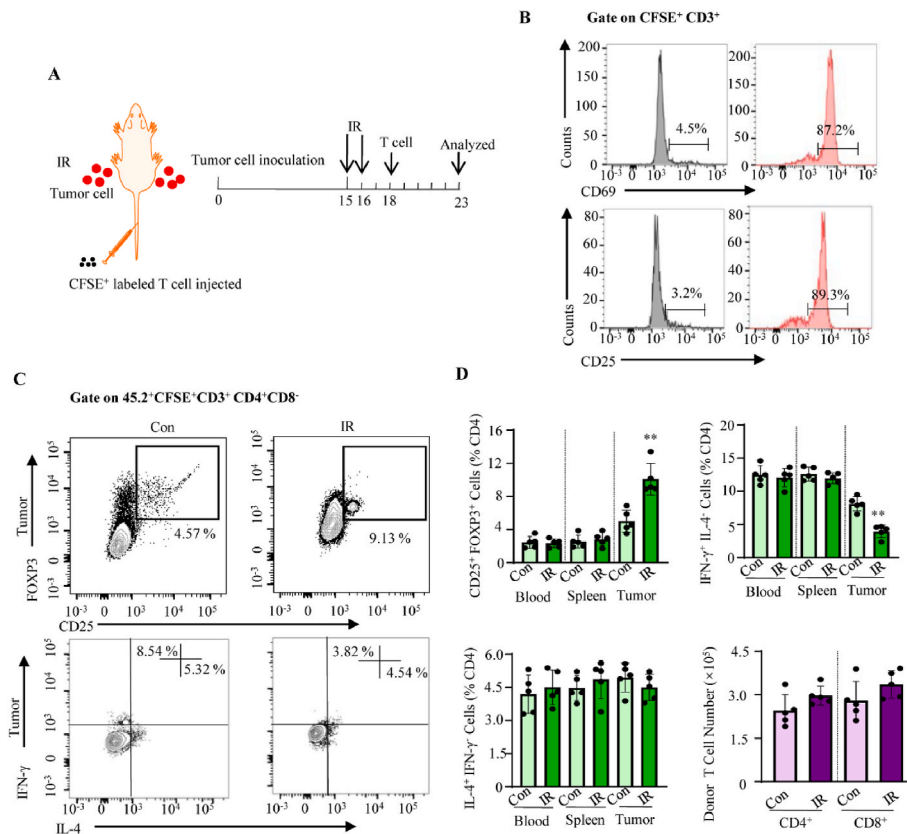
Fig. 2. Irradiated glioblastoma (GBM) cells decrease Th1 and increase Treg cells *in vivo*. (**A**) Schematic illustration of the treatment schedule. (**B**) Activated T cell markers CD69 and CD25 were tested using flow cytometry before they were injected into mice. (**C–D**) The T cell subsets in blood, spleens, and tumors from mice were measured using flow cytometry. Representative flow plots of CD25$^+$ FoxP3$^+$ Treg and IFN-γ^+ IL-4$^-$ Th1 in the tumor at 5 days after injection (**C**); The percentage of T cell subsets in the blood, spleens, and tumors from mice (**D**) (n = 6, IR: irradiation, **P < 0.01 *vs.* the control).

using PCR or real-time PCR.

2.17. Transient luciferase reporter assays

Various B7–H4 promoter fragments were synthesized and cloned into the pGL3-basic firefly luciferase reporter vector (Promega, Madison, WI, USA). Briefly, cells were seeded in 24-well plates for 24 h and transfected in triplicates with 0.5 μg of each experimental plasmid and 0.5 μg of the Renilla pRL-TK plasmid (used as a control) per well using Lipofectamine 3000, following the manufacturer's protocol. A dual-luciferase reporter assay (Promega) was performed to measure the relative luciferase activity 24 h after transfection. Relative light units (RLUs) from the firefly luciferase signals were normalized with the RLUs from Renilla luciferase signals.

2.18. Statistical analysis

All statistical analyses were performed using SPSS v.23.0 (IBM Corp., Armonk, NY, USA) or GraphPad Prism v8.0 (GraphPad Inc., La Jolla, CA, USA). Experimental data are presented as the mean ± SD. The means of two groups were compared using a two-sided Student's t-test, while means of multiple groups were compared using one-way ANOVA plus a two-sided Dunnett's test (when each group was compared with a control group) or a two-side Tukey's test (when each group was compared with every other group). Pearson Chi-Squared tests were used for correlation analysis. Survival curves were plotted using the Kaplan–Meier method and compared using log-rank tests. All P values are two-tailed and a P < 0.05 was considered statistically significant.

3. Results

3.1. Exosomes from irradiated GBM cells inhibit tumor infiltrating T cells' anti-tumor potential

To demonstrate the effects of exosomes from irradiated GBM cells on T cells, we first characterized the collected exosomes by NTA and immunoblotting analysis. The mode diameter of exosomes was 110.5 ± 26.7 nm, matching the reported size of typical exosomes [18] (Fig. S1A). They strongly expressed exosomal markers (CD63, CD81, ALIX and TSG101) but showed low expression of the mitochondrial marker (COX IV) and the endoplasmic reticulum (ER) markers (Calreticulin and Bip) (Fig. S1B). When T cells were treated with exosomes from irradiated GBM cells, decreased proinflammatory cytokines (IFN-γ and TNF-α) and increased anti-inflammatory cytokines (IL-1ra) were observed (Fig. 1A and B). Moreover, these effects were observed in a radiation dose-dependent manner (Fig. 1C and D). Examining the relative proportions of T cell subsets showed decreased proportions of IFN-γ$^+$ IL-4$^-$ Th1 cells and increased CD4$^+$ CD25$^+$ FoxP3$^+$ Tregs after exosomes treatment (Fig. 1E and F). However, the proportions of Th2, total CD4$^+$ or CD8$^+$, central memory CD4$^+$ or CD8$^+$, effector memory CD4$^+$, or CD8$^+$ T cells did not change (Fig. S2). Finally, western blotting analyses of Treg and Th1 transcription factors showed significantly reduced levels of T-bet and increased levels of Foxp3 in T cells treated with exosomes from irradiated GBM cells compared with those in the control group (Fig. 1G and H). Taken together, exosomes from irradiated GBM cells inhibit tumor infiltrating T cells' anti-tumor potential *in vitro*.

To investigate whether the irradiation-induced changes in GBM cells affect tumor-infiltrating T cells, mice bearing tumors after irradiation were injected with activated T cells purified from mice spleens (Fig. 2A). Flow cytometry showed that the majority of activated T cells expressed the activation markers CD69 and CD25 (Fig. 2B). Then, activated T cells were CFSE-labeled and injected into mice 48 h after tumor irradiation or
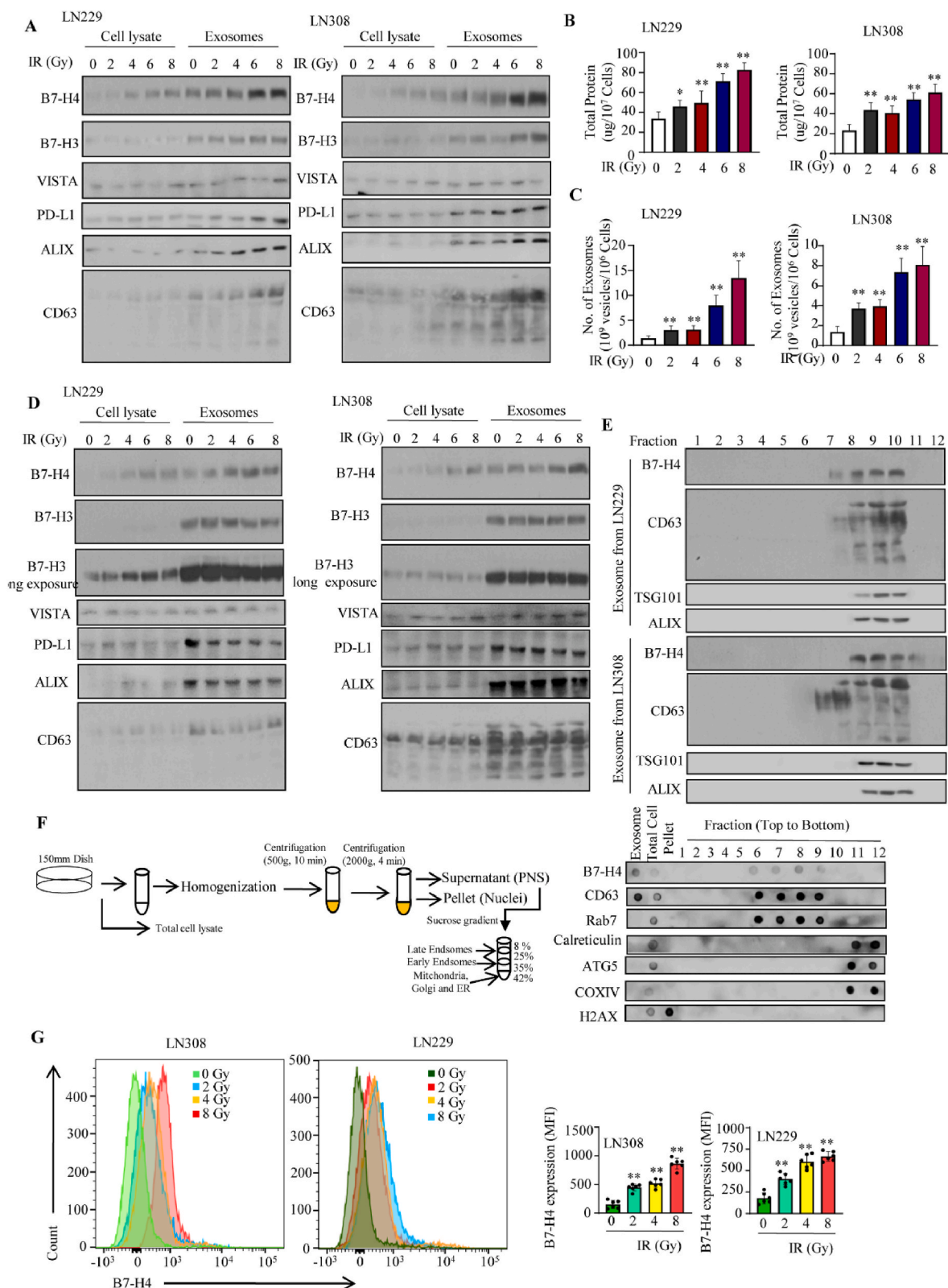
Fig. 3. Irradiation increased the production of exosomes and the level of B7–H4 in exosomes. (**A**) Exosomes from equal numbers of cells were tested by western blotting to detect various proteins, including exosomal markers and immune checkpoints. The antibody against B7–H4 (Cat# 252,438, Abcam, Cambridge, MA, USA) was used. (**B**) Protein concentration from equal numbers of cell was measured. (**C**) The number of exosomes from irradiated glioblastoma (GBM) cell culture supernatants was analyzed using nanoparticle tracking analysis (NTA) (n = 3) (Fig. S3C). (**D**) Proteins from equal amounts of total exosomes were measured using western blotting. (**E**) Density gradient centrifugation confirming that B7–H4 secreted by irradiated GBM cells co-fractionated with exosome markers CD63, ALIX, and TSG101. (**F**) Iodixanol density gradient centrifugation analysis showing that B7–H4 co-fractionated with exosome marker CD63 and late endosome marker Rab7. (**G**) The intracellular localization of B7–H4 was examined using flow cytometry (n = 6). (IR: irradiation; $*P < 0.05$, $**P < 0.01$ *vs.* the control).
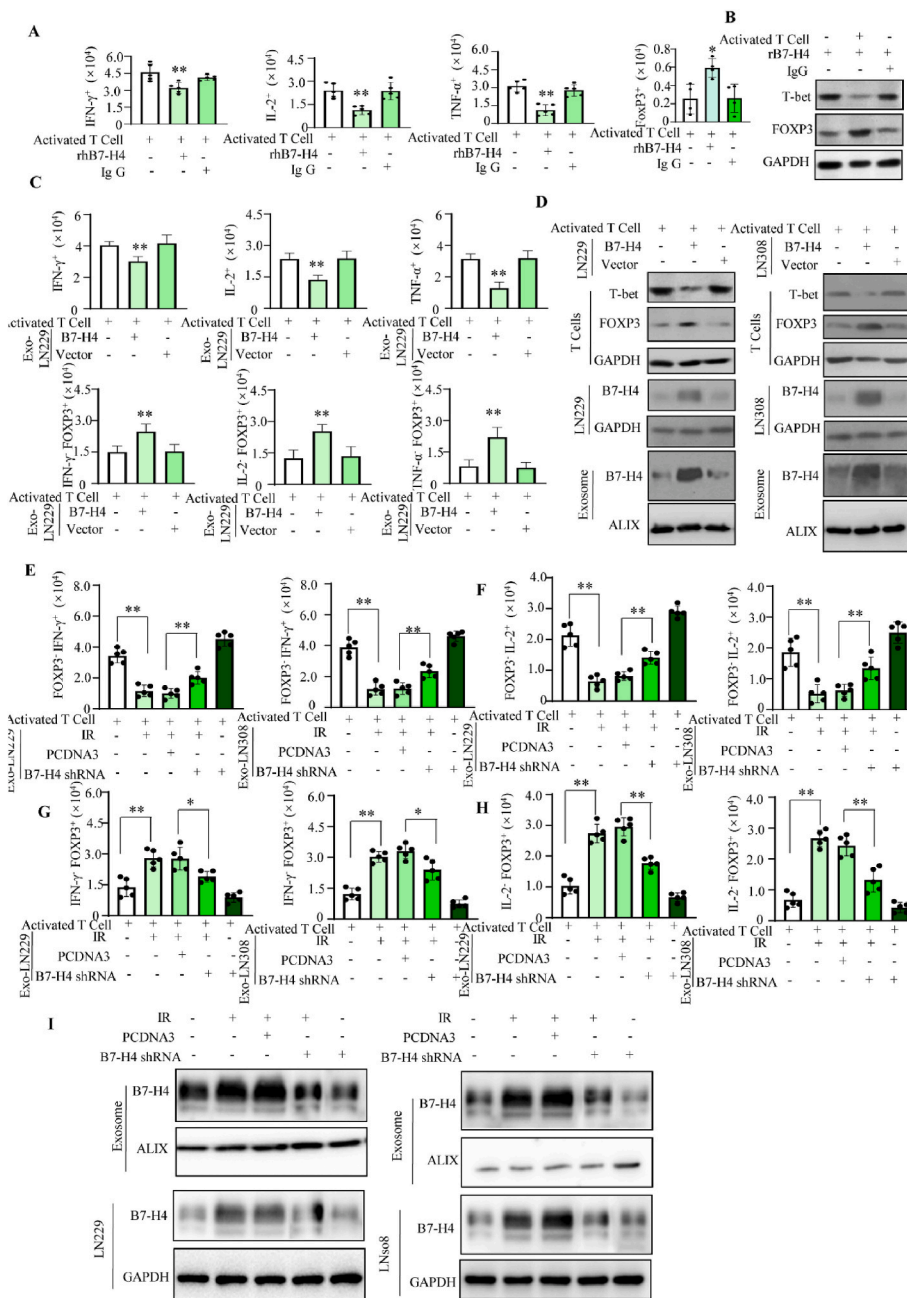
Fig. 4. Exosomal B7–H4 from irradiated glioblastoma (GBM) cells induces FoxP3 expression during Th1 cell differentiation. (**A - B**) Naïve T cells were activated and cultured in Th1 differentiation medium for 72 h, with or without the presence of immobilized rhB7-H4 at 100 ng/mL. (**A**) The expression of IFN-γ$^+$, IL-2$^+$, TNF-α$^+$, and FoxP3$^+$ cells were measured using flow cytometry assays; (**B**) The levels of T-bet and FoxP3 was measured using western blotting. (**C–D**) Naïve T cells were activated and cultured in Th1 differentiation medium for 72 h with exosomes from GBM cells expressing exogenous B7–H4 or vector. (**C**) The expression levels of IFN-γ, IL-2, TNF-α, and FoxP3 were tested by flow cytometry. (**D**) The levels of T-bet and FoxP3 were measured using western blotting. (**E–H**) The total number of FoxP3$^-$ IFN-γ$^+$, FoxP3$^-$ IL-2$^+$, FoxP3$^+$ IFN-γ$^-$, and FoxP3$^+$ IL-2$^-$ Th1 cells were measured when naïve T cells were treated by exosome from irradiated GBM cells, with or without B7–H4 shRNA. (**I**) The expression of B7–H4 in cells was validated by western blotting. (n = 5; IR: irradiation; Exo: exosomes. *$P < 0.05$ *vs.* the control; **$P < 0.01$ *vs.* the control).

mock treatment. After sacrifice, the number of adoptively transferred T cells infiltrating the spleen, blood and tumors were measured. Five days after T-cell transfer, increased proportions of Tregs and decreased Th1 cells were observed in the tumors of the irradiated group compared with control group. However, no significant difference in the proportions of Treg and Th1 cells in blood and spleen were observed between the two groups (Fig. 2C and D). Thus, the *in vitro* and *in vivo* data indicated that exosomes from irradiated GBM cells inhibit the T cells' anti-tumor immune response.

3.2. Increasing exosomal B7–H4 expression from irradiated GBM cells contributes to increased FoxP3 expression in differentiating Th1 cells

To investigate the role of irradiation of GBM cells secreting exosomal B7–H4, the size and number distribution were analyzed. Results showed that irradiation increased the total protein and the protein markers expression of exosomes from the same number of cells. Moreover, NTA showed that irradiation promoted exosome production without affecting their size distribution (Fig. 3A–C and Figs. S3A–C). Next, we analyzed immune checkpoint proteins carried by exosomes. The results revealed significantly higher levels of B7–H4, PD-L1, and B7–H3 in exosomes from irradiated cells than in exosomes from the same number of control cells (Fig. 3A and Figs. S3A and B). The expression of these proteins in the same amounts of exosomes were measured, which showed that the levels of B7–H4 were significantly higher, but there was no significant difference in B7–H3 and PD-L1 levels, in exosomes derived from irradiated cells compared to control cells (Fig. 3D and Fig. S3D). Iodixanol density gradient centrifugation confirmed that B7–H4 co-localized with ALIX (exosome) and Rab7 (late endosome) in irradiated GBM cells (Fig. 3F and Fig. S3E). Moreover, irradiation-upregulated B7–H4 was localized to the cell membrane (Fig. 3G). These data indicated indirectly that B7–H4 was carried by exosomes. Next, the clinical significance of B7–H4 expression was examined in 166 primary GBM tissues (Table S1), which showed that high B7–H4
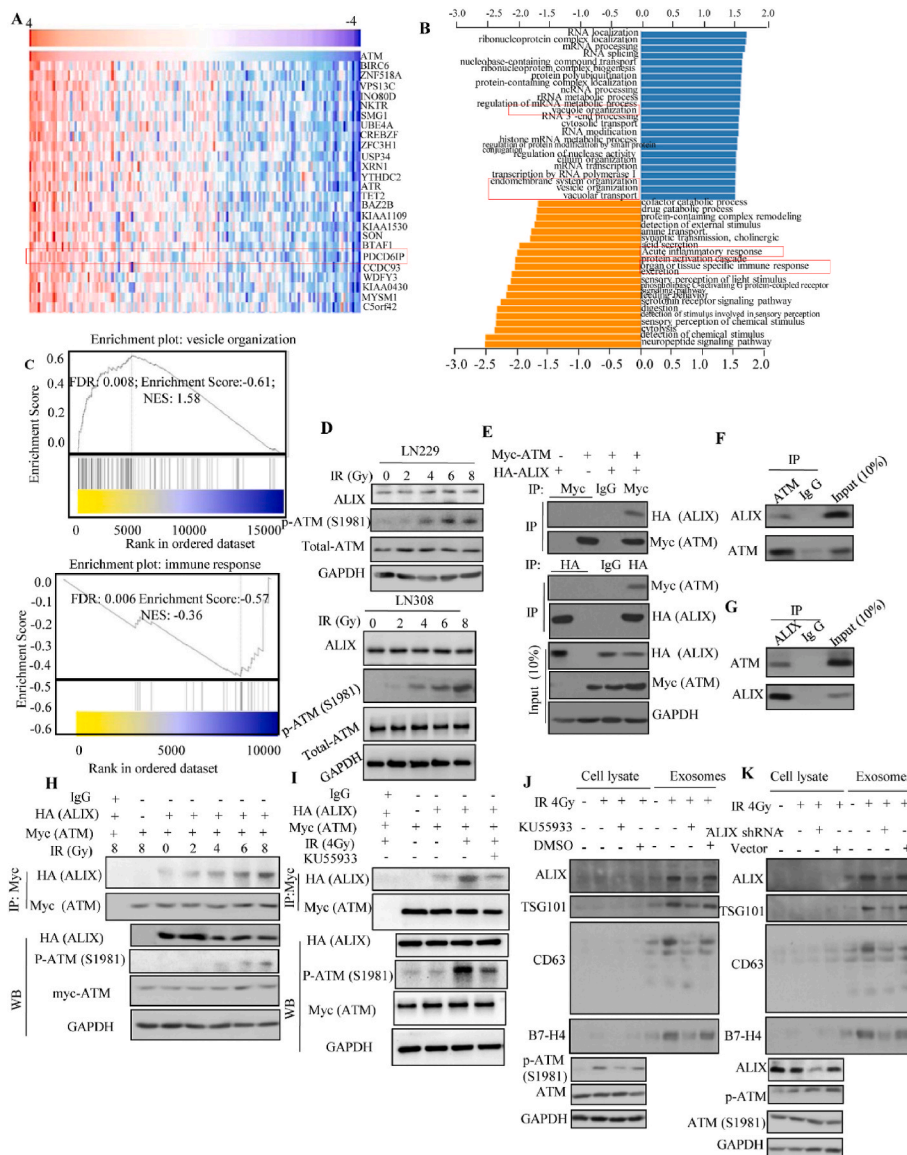
Fig. 5. Irradiation promotes the production of exosomes by increasing the interaction of phosphorylated ATM (*p*-ATM) with ALIX. (**A**) The top 26 significant genes that correlate positively with ATM in GBM are shown in heat maps. (**B**) The genes correlated with ATM were subjected to KEGG pathway analysis. (**C**) Enrichment plots from GSEA showing that vesicle organization and immune response were differentially enriched in the high ATM expression phenotype. (**D**) The levels of ALIX and *p*-ATM in irradiated GBM cells were measured using western blotting. (**E**) ALIX and ATM interact with each other. Myc-ATM and/or HA-ALIX were overexpressed in HEK293T cells. Co-IP was performed by incubating whole-cell lysates (200 µg) with either an anti-Myc or anti-HA antibodies (top and middle). Endogenous ALIX and ATM interact with each other in LN229 (**F**) and GBM tissue (**G**) were validated by Co-IP assay. (**H**) irradiation enhances the ATM–ALIX complex. ALIX and ATM were co-expressed in HEK293T cells for 24 h. The whole-cellular lysates (200 µg) were immunoprecipitated using an anti-Myc antibody, and the precipitates were detected using an anti-HA antibody. (**I**) KU55993 blocks the irradiation-induced formation of ALIX-ATM complexes. HEK293T cells were treated by KU55993, and Co-IP was performed by incubating whole-cell lysates (200 µg) with an anti-Myc antibodies. (**J** and **K**) The production of exosomes from irradiated LN229 cells treated by KU55993 (**J**) or *ALIX* shRNA (**K**) was measured by western blotting for exosomal markers. Exosomes were purified from equal number of cells and an equal volume of cell culture.

expression was associated with poor patient OS and progression-free survival (PFS) (Figs. S3F–H and Tables S2 and S3). These data indicated that radiation increased exosomal B7–H4 levels, which might be used as a predictor of poor prognosis in GBM.

To evaluate the effect of exosomal B7–H4 on Th1 cell biology directly, we measured the proliferation and apoptosis of Th1 cells treated with exosomes. Exosomes derived from irradiated GBM cells, with or without the *B7–H4* shRNA plasmid, did not affect the proliferation or apoptosis of Th1 cells (Figs. S4A–D). Thus, we hypothesized that exosomal B7–H4 might regulate Th1 cell differentiation. Naïve T cells isolated from PBMCs were activated and cultured with different Th1 differentiation media. Exposure to rhB7-H4 or exosome from GBM cells with *B7–H4* overexpression decreased IFN-γ, IL-2, TNF-α and T-bet expression significantly, increased levels of FoxP3 (Fig. 4A–D). Treating differentiating Th1 cells with exosomes from irradiated GBM cells led to a significant increase in FoxP3+ Th1 cells and a decrease in IFN-γ+ and IL-2+ Th1 cells. Moreover, *B7–H4* knockdown partially abrogated the induction of Foxp3 by exosomes from irradiated GBM cells (Fig. 4E–I). Collectively, these data indicated that increasing exosomal B7–H4 levels from irradiated GBM cells contribute to Foxp3 induction during Th1 cell differentiation.

3.3. Irradiation increases exosome production by enhancing the interaction of ATM with ALIX

The apical kinase, ATM, orchestrates the cellular responses to DNA damage produced by irradiation [19]. To determnine the involvement of ATM in exosome production, ATM-related genes from 153 GBM samples in the TCGA dataset were analyzed. *ATM* expression was positively correlated with about 2500 genes and negatively correlated with about 3100 genes. Among them, *ALIX*, which encodes for an important protein for exosomes biogenesis, correlated positively with *ATM* expression (Fig. 5A). Furthermore, to identify the significantly enriched pathways in the DEGs identified, KEGG pathway analysis was performed. Our results revealed that acute inflammatory response, organ or tissue-specific immune response, endomembrane system organization, vesicle organization, vacuolar transport, and vacuole organization were the significantly enriched pathways identified (Fig. 5B and C and Figs. S5A–C). To evaluate the role of ALIX in GBM samples from the CGGA and TCGA databases were analyzed, revealing that *ALIX* expression was higher in GBM compared with that in low grade glioma (LGG) (Fig. S5D). More importantly, *ALIX* upregulation tended towards a poor prognosis for patients with glioma (Figs. S5E–G). Furthermore, Pearson's correlation analysis showed positive correlations between *ATM*
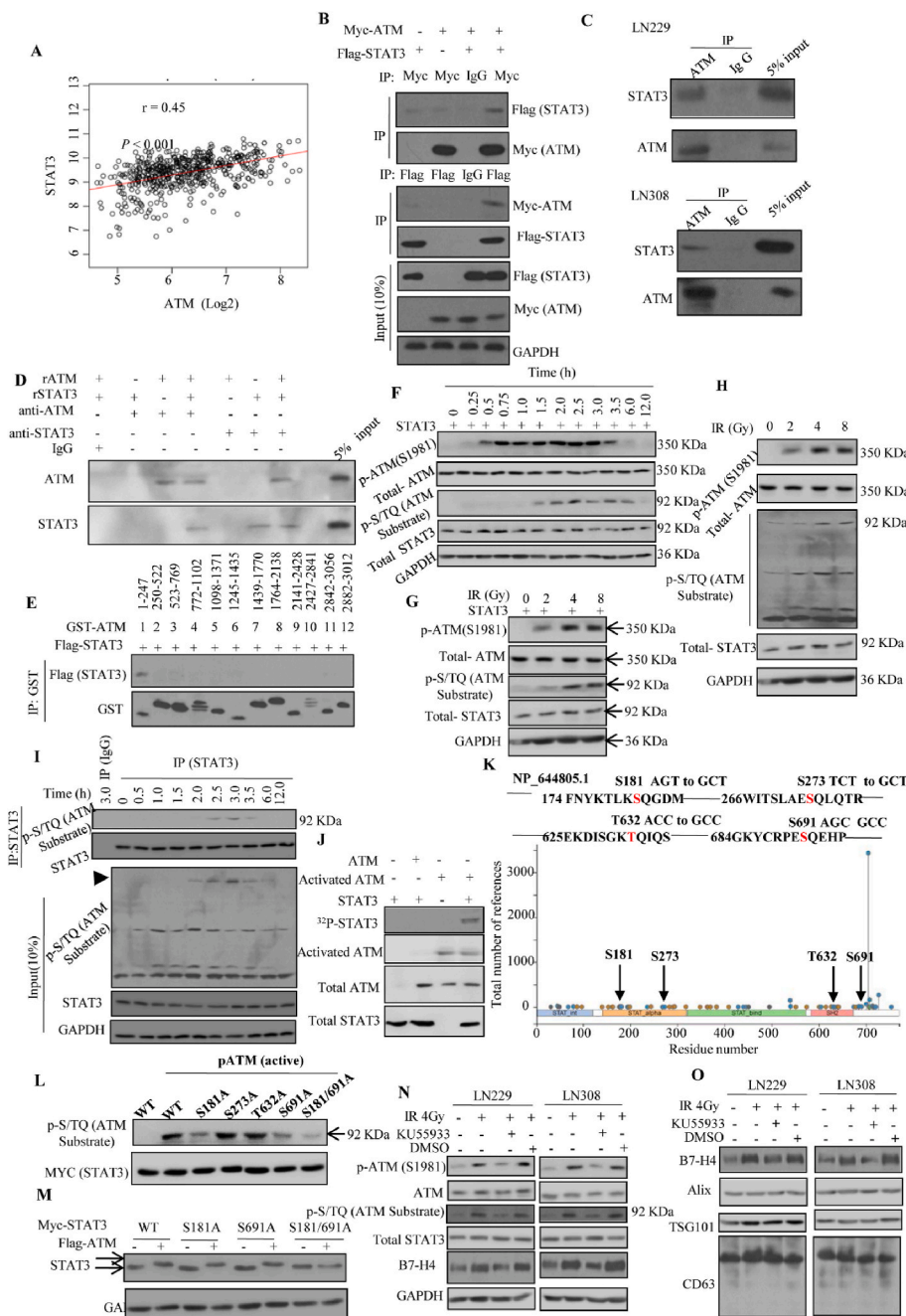
Fig. 6. Irradiation induces phosphorylation of STAT3 through ATM and increases the expression of exosomal B7–H4. (**A**) The interaction between *ATM* and *STAT3* was analyzed using Pearson's correlation analysis based on TCGA database. (**B**) Myc-ATM and/or Flag-STAT3 were overexpressed in HEK293T cells. Co-IP was performed by incubating whole-cell lysates (200 μg) with either an anti-Myc or anti-Flag antibodies (top and middle). (**C**) Endogenous ATM and STAT3 interact with each other in LN229 (upper panel) and LN308 (lower panel) cell lines. Co-IP was performed by incubating whole-cell lysates (500 μg) with anti-ATM antibodies, and the precipitates were detected using anti-STAT3 antibodies. (**D**) rATM and rSTAT3 interact with each other *in vitro*. rATM (50 ng) was incubated with rSTAT3 in IP buffer at 4 °C for 2 h, and pull down assays were performed. (**E**) GST-tagged ATM fragments were incubated with lysates from HEK293T cell overexpressing FLAG-STAT3 for the GST pull down assay. (**F–H**) A 92-kDa protein band in which STAT3 mainly located was significantly apparent in cells after irradiation (IR). (**F**) LN229 cells with exogenous STAT3 expression were treated with IR at 4 Gy and investigated at the indicated time points. (**G** and **H**) LN229 cells with (**G**) or without (**H**) the *STAT3* overexpression vector were treated with IR at the indicated doses. (**I**) LN229 cells treated with IR at 4 Gy were measured at the indicated times by co-IP assay. (**J**) Phosphorylation of purified STAT3 protein by ATM *in vitro*. (**K**) The candidate STAT3 sites phosphorylated by ATM were identified using the online tool PhosphoSitePlus (https://www.phosphosite.org/). (**L-M**) ATM phosphorylates STAT3 at S181 and S691. STAT3 WT and various mutants were expressed and immunoprecipitated. The precipitates were incubated with a purified active pATM in *in vitro* kinase assay. (**M**) Mutation of STAT3 at S181/S691 blocked the ATM – induced shift in STAT3 migration. (**N–O**) Total cell lysate and exosomal lysate were assessed using western blotting. The ATM kinase inhibitor KU55933 prevented the irradiation-induced STAT3 phosphorylation in GBM cells (**N**). (**O**) ATM inhibitor KU55933 prevented irradiation-induced exosomal B7–H4 expression.

and *ALIX* mRNA expression levels in GBM tissues (Figs. S5H and I). ALIX expression was also examined in 166 GBM tissue samples. Our results showed that patients with low ALIX expression levels had longer OS and PFS (Fig. S5J,**K** and Table S4). Taken together, these data supported the association between ATM and ALIX.

To further investigate the role of ATM and ALIX in radiation-induced exosome production, ATM and ALIX levels in GBM cells after irradiation was measured. However, no significant change was observed when GBM cells were irradiated (Fig. 5D). Our IP experiments showed that ALIX and ATM interacted directly with each other (Fig. 5E–G). Furthermore, irradiation increased the interaction of ALIX with ATM in a dose dependent manner (Fig. 5H), which could be reversed by using the ATM kinase inhibitor, KU55933 (Fig. 5I). We then investigated whether the exosome production was affected by ATM and ALIX. The results revealed that exosome production increased by irradiation, and this effect can be partly abolished by KU55933 or *ALIX* shRNA (Fig. 5J, K).

These results indicated that irradiation increased exosome production by partly enhancing the interaction of phosphorylated ATM with ALIX.

3.4. Irradiation induces phosphorylation of STAT3 by ATM and increases exosomal B7–H4 levels

Analysis of the TCGA dataset showed that the ATM-associated DEGs were enriched in the acute inflammatory response and immune response signaling pathways (Fig. 5B, C and Fig. S5C). Moreover, previous studies confirmed that activated STAT3 could promote B7–H4 expression [20]. Thus, we hypothesized that irradiation might increase B7–H4 expression via ATM-phosphorylated STAT3. Firstly, an analysis of the TCGA dataset showed that *ATM* expression correlated positively with *STAT3* expression (Fig. 6A). Next, analyzing the gene expression profiles of WHO grade I–IV glioma tissues showed that *STAT3* expression increased with higher tumor stage (Fig. S6A, **B**). Moreover, high *STAT3* expression
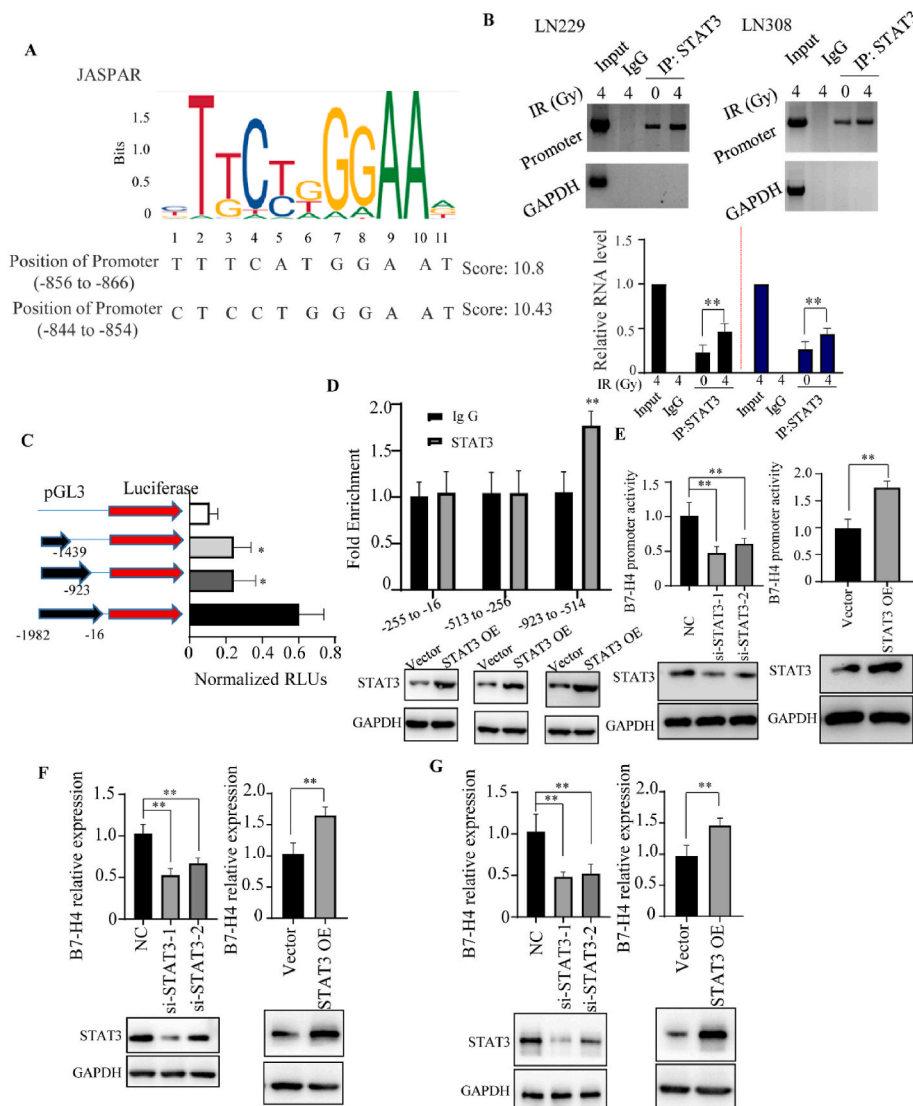
Fig. 7. STAT3 binds to the *B7–H4* promoter and upregulates B7-H4 expression in glioblastoma (GBM) cells. (**A**) The position of the most representative putative binding sites of the promoter associated with STAT3 motifs predicted by JASPAR (http://jaspar.genereg.net). (**B**) Binding of STAT3 to the *B7–H4* promoter was examined by chromatin immunoprecipitation (ChIP) PCR assay. (**C**) Activity of the different fragments of the *B7–H4* promoter was determined using a dual-luciferase assay. Results are presented as normalized relative luciferase units (RLUs); n = 3 independent experiments. (**D**) Binding of STAT3 to the *B7–H4* promoter was examined by ChIP-qPCR. (**E**) *B7–H4* promoter activity in LN229 cells transiently transfected with control siRNA (NC), *STAT3* siRNAs (si-STAT3-1, si-STAT3-2), control plasmid for STAT3 (vector), or a *STAT3* overexpression plasmid (STAT3 OE), was measured using a dual-luciferase assay. (**F** and **G**) *B7–H4* mRNA levels in LN229 (**F**) and LN308 (**G**) cells with transient *STAT3* knockdown or overexpression was detected. (n = 3; *$P < 0.05$ *vs.* the control; **$P < 0.01$ *vs.* the control).

indicated poor OS and PFS in GBM patients (Fig. S6C, **D**). To support these findings, STAT3 expression was examined in GBM tissues using IHC, which showed that tumor STAT3 levels correlated inversely with PFS and OS (Figs. S6E–G and Table S5). Consistently, univariate and multivariate analyses confirmed that STAT3 overexpression was significantly associated with poor OS and PFS (Table S3). Collectively, these data indicated that STAT3 was associated with poor disease outcome.

To test whether ATM interacts directly with STAT3, co-IP assays were performed, which indicated that ATM and STAT3 interacted with each other in cellular lysates (Fig. 6B and C). Co-incubation of purified ATM and STAT3 also confirmed their direct interaction (Fig. 6D). Further study indicated that GST–ATM1 (amino acid residues 1–247) interacted robustly with STAT3 *in vitro* (Fig. 6E). To investigate the phosphorylation status of STAT3, proteins from indicated GBM cells were subjected to western blotting using a p-S/TQ (ATM Substrate) antibody. ATM phosphorylation increased at 0.5 h and decreased at 3.5 h, whereas the phosphorylation of STAT3 occurred later. Moreover, irradiated human GBM cells with exogenous or endogenous STAT3 showed a radiation dose-dependent increase in STAT3 phosphorylation (Fig. 6F–H and **S6H, I**). Similarly, IP assays demonstrated an increase in STAT3 phosphorylation upon irradiation of a GBM cell line (Fig. 6I). Interestingly, *in vitro* kinase assays demonstrated that activated ATM immunoprecipitated from HEK-293T cell lysates directly phosphorylated purified STAT3 (Fig. 6J). In line with this, four candidate STAT3

phosphorylation sites (SQ/TQ motifs) at S181, S273, T632, and S691 were predicted by PhosphoSitePlus (Fig. 6K). Mutation analysis identified that the S181A and S691 mutations led to decreased phosphorylation and a shift in STAT3 migration; phosphorylation was totally absent in the double mutant (S181/691A; Fig. 6L, **M**). Consistently, the ATM inhibitor prevented the radiation-induced STAT3 phosphorylation (Fig. 6N). Furthermore, STAT3 downregulation also decreased B7–H4 induction in response to irradiation (Fig. S6J). Moreover, the ATM inhibitor decreased the exosomal B7–H4 level (Fig. 6O). Overall, these results demonstrated that irradiation induced ATM phosphorylation of STAT3 and increased B7–H4 expression.

Next, we investigated the molecular mechanism underlying the positive correlation between STAT3 and B7–H4 levels in GBM cells. JASPAR analysis of the *B7–H4* promoter identified several putative STAT3 binding sites (Fig. 7A). ChIP assays revealed the direct binding of STAT3 to the *B7–H4* promoter region. Moreover, the level of B7–H4 promoter binding to STAT3 was increased upon irradiation (Fig. 7B). Similarly, dual luciferase reporter assays using reporter plasmids bearing the different lengths of the core promoter region of *B7–H4* suggested that the $-923 \sim -16$ bp region was critical for *B–7H4* promoter activity (Fig. 7C). Consistent with this finding, ChIP assays showed that STAT3 binds mainly at the $-923 \sim -514$ bp region of the *B7–H4* promoter (Fig. 7D). Conversely, *B7–H4* promoter activity was decreased upon small interfering RNA (si-RNA)-mediated *STAT3*
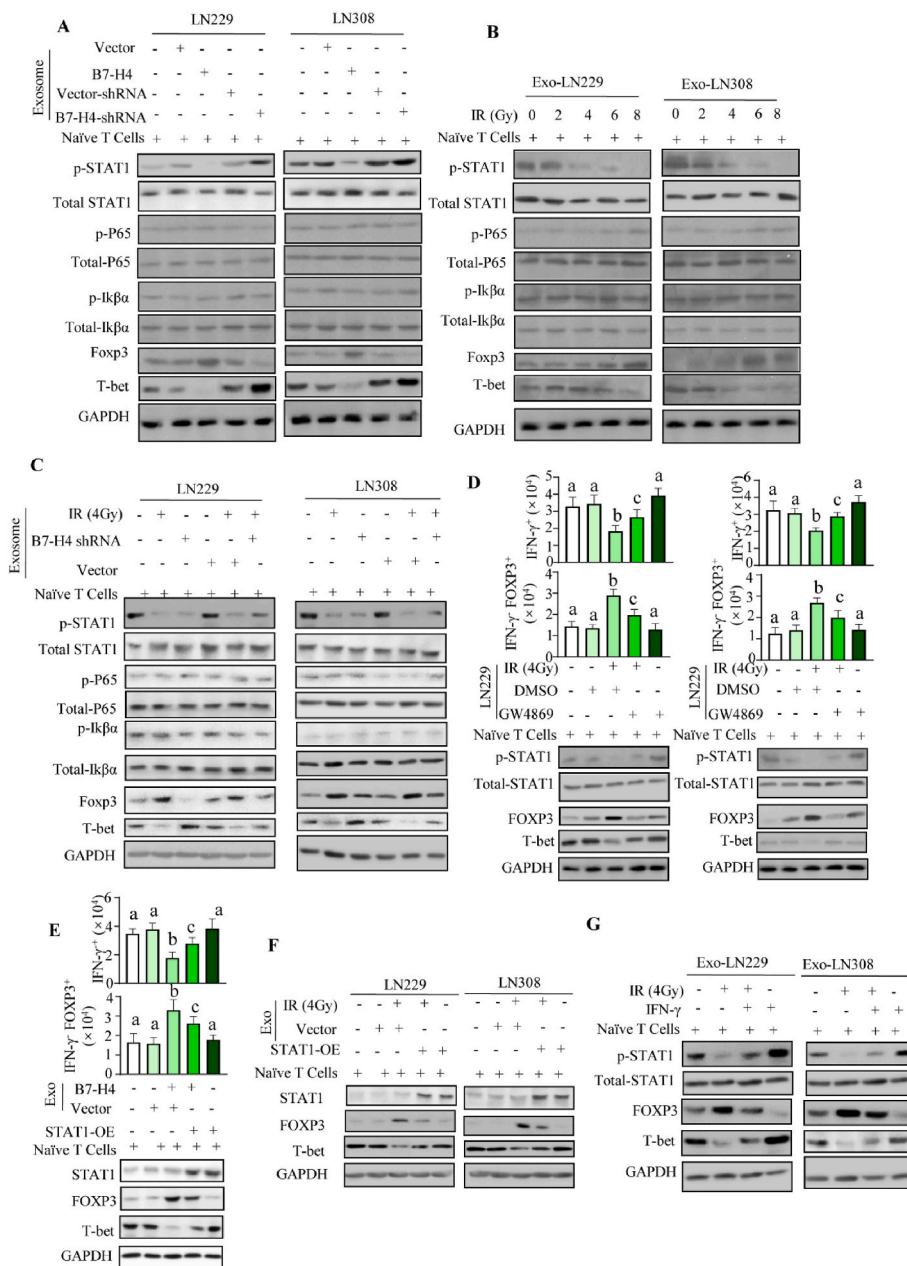
Fig. 8. Exosomal B7–H4 reduces Th1 cell differentiation via STAT1 pathway activation. (**A**) Naïve T cells cultured in Th1 differentiation medium supplemented with exosomes from GBM cells transfected with B7–H4, or B7–H4 shRNA plasmids. Then, members of the IFN-γ/STAT1 pathway and NF-κβ pathway were evaluated using western blotting. (**B**) Naïve T cells were activated and cultured in Th1 differentiation medium supplemented with exosomes from irradiated GBM cells. The key proteins associated with NF-κβ (Ikβα and P65) and the IFN-γ/STAT1 pathway were detected by western blotting (**C**) The levels of phosphorylated STAT1, FoxP3, and T-bet in Th1 cells were measured. (**D**) Flow cytometry assessment of the total number of IFN-γ⁻ FoxP3⁺, and IFN-γ⁺ Th1 cells treated by exosomes from GBM cells with irradiation (IR) or IR plus GW4869 (upper panel). STAT1 activation, and T-bet and FoxP3 levels were evaluated using Western blot in Th1 cells. (**E**) Naïve T cells overexpressing *STAT1* were treated using exosomes from LN229 cells with exogenous B7–H4, and the total number of IFN-γ⁻ FoxP3⁺ and IFN-γ⁺ Th1 cells were measured using flow cytometry and the levels of FoxP3 and T-bet was investigated using western blotting. (**F**) The levels of STAT1, FoxP3, and T-bet in Th1 cells was measured using Western blot. (**G**) Western blot was used to investigate the levels of STAT1, FoxP3, and T-bet in exosome-treated T cells re-stimulated by IFN-γ. (n = 3; Bars with different characters are statistically different at the $P < 0.05$ level).

knockdown, but was enhanced by *STAT3* overexpression (Fig. 7E). Correspondingly, *B7–H4* mRNA levels decreased in GBM cells after *STAT3* knockdown, but increased after *STAT3* overexpression (Fig. 7F and G). These results exhibited that irradiation induced the phosphorylation of STAT3 by ATM and increased the level of STAT3 binding to the *B7–H4* promoter to upregulate *B7–H4* expression.

3.5. Exosomal B7–H4 increase FoxP3 expression in differentiating Th1 cells via STAT1 pathway inactivation

Given our current findings, we set to find out how exosomal B7–H4 induces FoxP3 expression during Th1 cell differentiation. First, RNA-sequencing data from TCGA glioma samples were analyzed and the differential gene expression based on B7–H4 status was summarized in a heatmap (Fig. S7A). GO analysis showed that the most significant biological process, cellular location, and molecular function subcategories were biological regulation, membrane binding, and protein binding, respectively (Fig. S7B). Meanwhile, KEGG analysis showed significant

enrichment of terms involving double-strand break repair, cell cycle G2/M phase transition, I-kappa B kinase/nuclear factor kappa-B (NF-κβ) signaling, and IFN-γ response (Figs. S7C–E). Thus, the levels of key proteins in the immune response-associated NF-κβ and IFN-γ pathways were determined. The results showed increased STAT1 phosphorylation, but not p65 and IKβα phosphorylation, in T cells treated with exosomes derived from *B7–H4* overexpression cells compared with those from the control group (Fig. 8A). Importantly, TCGA dataset analysis showed that upregulated *STAT1* was associated with poor prognosis of LGG patients (Fig. S7F). Decreased STAT1 phosphorylation and increased FoxP3 levels were observed in differentiating Th1 cells treated by exosomes from irradiated GBM cells (Fig. 8B), which could be abolished by depletion of B7–H4 (Fig. 8C). Moreover, the inhibitor of exosome release GW4869 partially reversed the decreased p-STAT1 and decreased FoxP3 expression in T cells cocultured with irradiated cells (Fig. 8D).

To further investigate the role of STAT1 in the immune response, purified T cells transfected with STAT1 plasmids were co-cultured with *B7–H4* overexpressing or irradiated cells. STAT1 overexpression
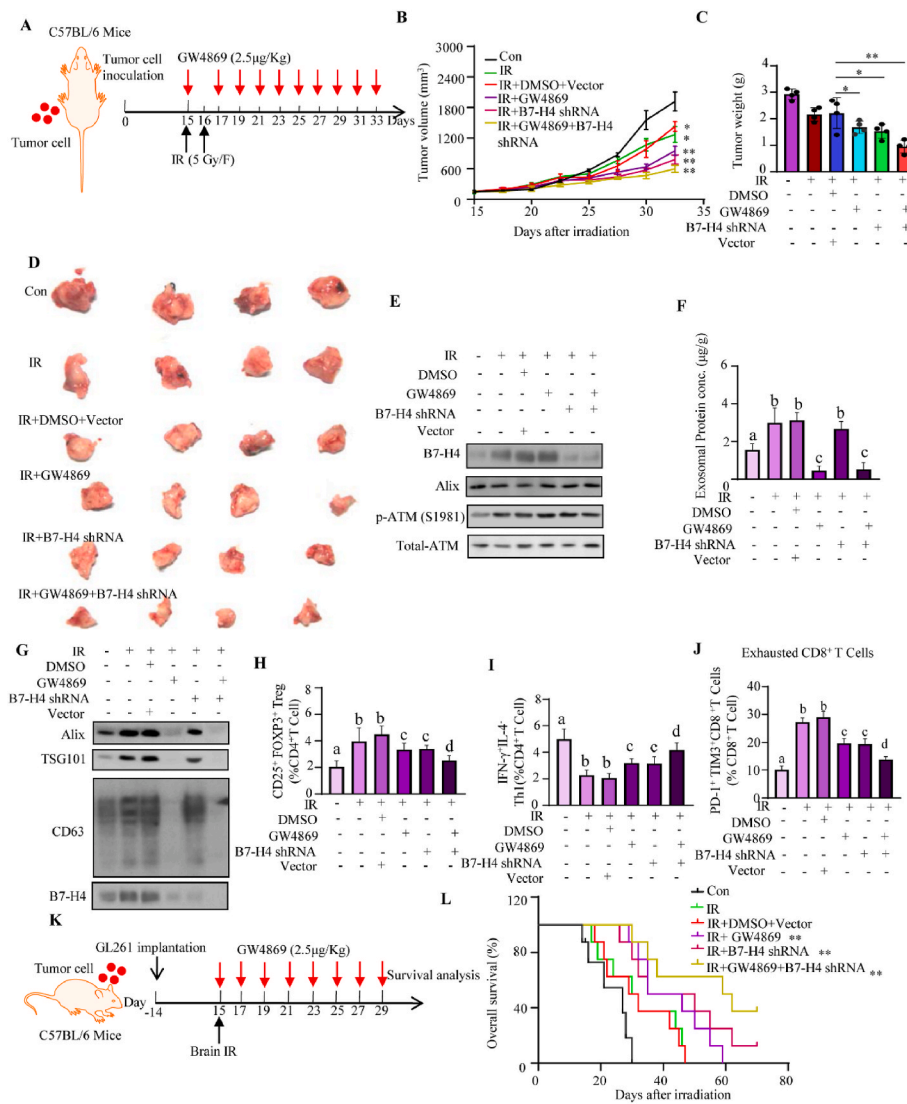
Fig. 9. Exosomal B7–H4 decreases the radiosensitivity of glioblastoma (GBM) cells, and reduces murine survival in the GL261 model. (**A**) To model the treatment of an established tumor, GL261 tumor-bearing mice were irradiated and injected intraperitoneally with GW4869. (**B**) The influence of exosomal B7–H4 on GL261 tumor growth in C57BL/6 mice (n = 4). (**C**) Histograms showing the mean tumor weights for each group. (**D**) Representative images of tumors are presented. (**E**) Western blotting analysis of B7–H4, *p*-ATM, and ALIX in the whole cell lysate extracted from xenografts. (**F**) The protein concentration from equal amounts of tumor tissue was measured using BCA. (**G**) The levels of B7–H4, ALIX, TSG101, and CD63 in exosomes purified from tumor tissue were measured using western blotting (equal tumor weight). (**H - J**) The downregulation of B7–H4 and injection of GW4869 decreased the proportion of CD4$^+$CD25$^+$FOXP3$^+$Treg cells, exhausted PD-1$^+$TIM-3$^+$ CD8$^+$T cells, and increased the proportion of IFN-γ^+IL-4$^-$ Th1 cells in tumors. (**K**) C57BL/6 mice were intracranially implanted with GL261 cells with exogenous B7–H4 or control vector. Then, GL261 tumor-bearing mice were irradiated and injected intraperitoneally with GW4869. (**L**) Overall survival analysis of mice bearing B7–H4 shRNA and/or injection GW4869 (n = 8). Bars with different characters are statistically different at the *P* < 0.05 level.

reverted the immune response inhibited by exosomes from *B7–H4* overexpressing cells or irradiated GBM cells, as indicated by the increased number of Th1 cells and T-bet protein levels (Fig. 8E, F). IFN-γ is critical for naive CD4$^+$ T cell differentiation towards Th1 and maintains the Th1 phenotype in a STAT1 activity-dependent manner [21]. We hypothesized that IFN-γ might revert Th1 cell polarity by phosphorylating STAT1. To test this hypothesis, exosome-treated Th1 cells were re-stimulated in the presence of IFN-γ. Consistently, IFN-γ increased STAT1 phosphorylation and T-bet levels, but decreased FoxP3 levels (Fig. 8G). These data indicated that exosomal B7–H4-mediated Th1 cells differentiate into regulatory T cells via STAT1 pathway inactivation.

3.6. Exosomal B7–H4 decreases GBM cell sensitivity to irradiation, and reduces murine survival in vivo

To explore the effect of exosomal B7–H4 on GBM radiosensitivity *in vivo*, GL261 cells transfected with *B7–H4* shRNA or control vector were transplanted s.c. into mice. Several days later, the mice were treated with radiotherapy and GW4869 (Fig. 9A). The results indicated that either injection of GW4869 or downregulation of *B7–H4* inhibited the growth of irradiated tumors significantly. Also, post-irradiation, tumors established by implantation of *B7–H4* downregulated cells treated by GW4869 displayed reduced growth compared with tumors treated with

the DMSO vehicle (Fig. 9B–D). Western blotting analysis of tumor tissues or exosomes indicated that the levels of exosomal markers and the protein concentration from equal tumor tissue were higher in irradiated tumors compared with those in control tumors. Moreover, irradiation increased the B7–H4 levels, especially exosomal B7–H4 levels. However, exosomal B7–H4 levels were downregulated by either *B7–H4* shRNA or GW4869 (Fig. 9E–G). Flow cytometry determination of T cell subsets in tumors showed that irradiation decreased the proportion of Th1 cells and increased the ratio of Treg cells, PD-1$^+$ TIM-3$^+$ exhausted CD8$^+$ T cells in tumors significantly, which could be partly reversed by GW4869 injection or *B7–H4* downregulation. *B7–H4* shRNA combined with GW4869 synergistically affected the proportion of T cell subsets (Fig. 9H-**J**). However, the proportions of CD4$^+$, CD8$^+$, Th1, Th2, and Treg cells in PBMCs and the spleen were unaffected (Figs. S8A–G), suggesting that exosomal B7–H4 suppresses anti-tumor immunity locally. We next examined whether *B7–H4* downregulation or GW4869 injection further extended murine survival. Using the treatment schedule shown in Fig. 9K, GL261 tumor-bearing mice with exogenous *B7–H4* shRNA or control vector were irradiated and treated with either GW4869 or DMSO. Mice bearing tumors treated with either *B7–H4* shRNA or GW4869 survived for longer than mice bearing control tumors. Compared with treatment by either *B7–H4* shRNA or GW4869 alone, the combination therapy extended survival, including long-term survivors that were not observed with either monotherapy (Fig. 9L).
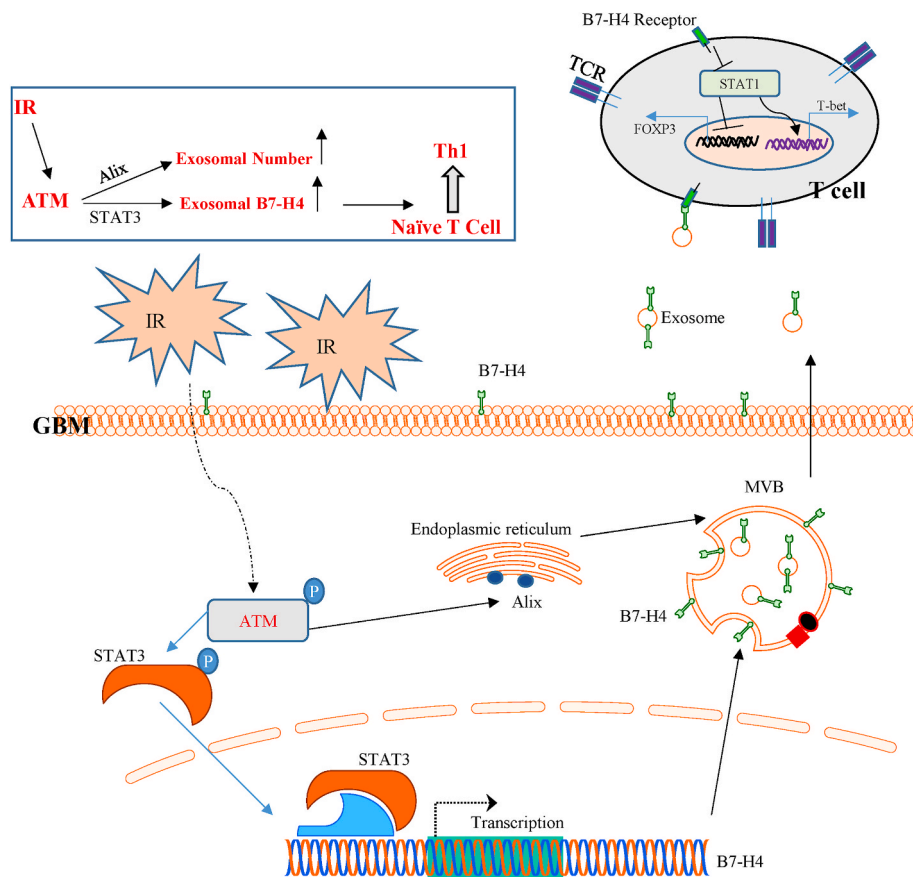
Fig. 10. Model of the contribution of exosomal B7–H4 from irradiated glioblastoma cells to immunosuppression and promotion of tumor growth.

These results suggested that B7–H4 decreases GBM radiosensitivity via exosomes. Finally, we performed the same *in vivo* experiment using T-cell immunodeficient BALB/c nude mice. Neither *B7–H4* shRNA nor GW4869 could increase GL261 cell radiosensitivity in these T-cell immunodeficient mice (Figs. S8H–J). Taken together, these results indicate that exosomal B7–H4 decreases GBM cell sensitivity to irradiation, and reduces murine survival in the GL261 model.

4. Discussion

Radiotherapy is the most important therapeutic weapon against GBM. The TME of GBM promotes tumorigenesis and the development of radio-resistance [6,7]. In this study, we examined the effect of radiation on tumor-infiltrating immune cells. We found that irradiated GBM cells inhibited anti-tumor immune responses of T cells and promoted tumor growth *in vitro* and *in vivo*. Mechanistically, irradiation promotes the production of exosomes by increasing the interaction of ATM and ALIX, and induces exosomal B7–H4 expression via STAT3 phosphorylation in GBM cells. Subsequent inactivation of STAT1 signaling by exosomal B7–H4 enhances Foxp3 expression during Th1 cell differentiation (Fig. 10).

Previous studies show that irradiation can enhance the local anti-tumor immune response and trigger an abscopal effect [8]. However, radiation might also induce immunosuppression by activating the non-canonical NF-kβ pathway or upregulating PD-L1 expression in tumor cells [22]. Moreover, irradiation could cause the accumulation of immunosuppressive cells including Treg in the TME, increased suppressive Tregs by promoting their proliferation [23]. The increased numbers of Tregs in tumors in response to localized irradiation might reflect the intrinsic radio-resistance of these cells [24]. Such findings are consistent with our result that irradiated GBM cells lead to a heightened immunosuppressive environment and subsequent tumor radio-resistance.

Exosomal PD-L1 levels correlate with disease progression of head and neck squamous cell carcinoma [10,18,25]. GL261 cell-released exosomes express PD-L1 on their surface and play an important role in blocking T cell activation and proliferation in response to T cell receptor stimulation [26]. The coinhibitory molecule B7–H4, which is overexpressed in many human cancers, is an important member of the B7/CD28 family. However, B7–H4's presence in cancer cell-derived exosomes and its role in tumor progression are largely unknown. Our results indicated that increased exosomal B7–H4 from irradiated GBM cells induces FoxP3 expression during Th1 cell differentiation. To our knowledge, no study has reported the involvement of tumor cell-derived exosomal B7–H4 in Th1 conversion to Tregs.

B7–H4 is upregulated in various types of cancers and is associated with poor clinical outcome [27]. *In vitro*, *B7–H4* is transcriptionally upregulated in cell lines in response to hypoxia and transforming growth factor β (TGF-β), via hypoxia inducible factor (HIF) 1α and STAT3 [20]. Functionally, B7–H4 overexpression in tumor cells plays a dominant role in inhibiting T cell antitumor responses through multiple pathways [27, 28]. Similarly, our results indicated that B7–H4 expression is associated with glioma grade and poor prognosis of GBM patients, partly by increasing FoxP3 expression during Th1 cell differentiation. Mechanistically, STAT3 binds to the *B7–H4* promoter and upregulates *B7–H4* expression in GBM cells. We speculated that B7–H4 could be a promising biomarker for immunotherapy in patients with glioma. Generally, when activated, the fate of naïve T cells is dictated by the cytokines they receive from the inflammatory milieu. Many factors can regulate Th1 differentiation and IFN-γ production [29,30]; however, the role of B7–H4 in Th1 differentiation was unknown. This study presents evidence that B7–H4 induces Foxp3 expression, which inhibits Th1 cell

differentiation, providing a mechanism for the effect of B7–H4 on T cell antitumor immune responses.

ATM kinase is required for PD-L1 upregulation in response to radiation-induced DNA damage [19,31]. However, the relationship between ATM signaling and B7–H4 expression in cancer cells is still unexplored. In this study, we showed that irradiation upregulates B7–H4 expression via the ATM/STAT3 signaling pathway. The transcription factor STAT3 is often upregulated in tumor cells and is a recognized negative prognostic factor [32]. Similarly, our results indicated that STAT3 expression is associated with poor survival. Further study indicated that ATM directly phosphorylates STAT3, increasing B7–H4 expression. Moreover, we showed that ATM phosphorylates STAT3 at S181 and S691 residues. However, the exact mechanism as to how phosphorylated STAT3 regulates its interaction with the *B–7H4* promoter warrants further studies. A deeper understanding of the molecular mechanism underlying B7–H4 expression in cancer cells may contribute to improve the efficacy of combined anti-B7-H4 therapy and radiotherapy.

Overall, the results of the present study showed that irradiated GBM cells inhibit the anti-tumor immune responses of T cells *in vitro* and *in vivo*. Mechanistically, irradiation promotes exosome production by increasing the interaction of ATM with ALIX, and induces the expression of exosomal B7–H4 via ATM-phosphorylated STAT3. In turn, the exosomal B7–H4 induces FoxP3 expression in differentiating Th1 cells via STAT1 pathway inactivation. However, some potential limitations in this study should be noted. Our findings support the co-administration of radiotherapy with anti-B7-H4 therapy to improve local tumor control. Furthermore, we provide a theoretical basis for exosomal B7–H4 as a potential tumor biomarker; however, further investigation in blood or cerebrospinal fluid is required.

Author contributions

Author contributions are listed as follows: Yunhong Tian, Chunshan Liu, Zhiyong Li, and Meiling Ai did the experiments and analyzed the data. Baiyao Wang, Kunpeng Du, Wei Liu, Hongmei Wang, Peng Yu, Chengcong Chen, Jie Lin, Anan Xu, and Rong Li participated in doing the experiments. Weijun Zhang, and Yawei Yuan conceived the idea of the study and did manuscript writing. All authors had access to the study data and approved the final manuscript.

Declaration of competing interest

None of the authors have conflicts of interest relevant to this article.

Data availability

Data will be made available on request.

Acknowledgements

Appendix A. Supplementary data

Supplementary data to this article can be found online at https://doi.org/10.1016/j.redox.2022.102454.

References

[1] Q.T. Ostrom, H. Gittleman, G. Truitt, A. Boscia, C. Kruchko, J.S. Barnholtz-Sloan, CBTRUS statistical report: primary brain and other central nervous system tumors diagnosed in the United States in 2011-2015, Neuro Oncol. 20 (2018) iv1–iv86.

[2] M.R. Gilbert, J.J. Dignam, T.S. Armstrong, J.S. Wefel, D.T. Blumenthal, M.A. Vogelbaum, et al., A randomized trial of bevacizumab for newly diagnosed glioblastoma, N. Engl. J. Med. 370 (2014) 699–708.

[3] R. Stupp, S. Taillibert, A.A. Kanner, S. Kesari, D.M. Steinberg, S.A. Toms, et al., Maintenance therapy with tumor-treating fields plus temozolomide vs temozolomide alone for glioblastoma: a randomized clinical trial, JAMA 314 (2015) 2535–2543.

[4] H.E. Barker, J.T. Paget, A.A. Khan, K.J. Harrington, The tumour microenvironment after radiotherapy: mechanisms of resistance and recurrence, Nat. Rev. Cancer 15 (2015) 409–425.

[5] M. McLaughlin, E.C. Patin, M. Pedersen, A. Wilkins, M.T. Dillon, A.A. Melcher, et al., Inflammatory microenvironment remodelling by tumour cells after radiotherapy, Nat. Rev. Cancer 20 (2020) 203–217.

[6] E.J. Sayour, P. McLendon, R. McLendon, G. De Leon, R. Reynolds, J. Kresak, et al., Increased proportion of FoxP3+ regulatory T cells in tumor infiltrating lymphocytes is associated with tumor recurrence and reduced survival in patients with glioblastoma. Cancer immunology, immunotherapy, CII 64 (2015) 419–427.

[7] A. Gieryng, D. Pszczolkowska, K.A. Walentynowicz, W.D. Rajan, B. Kaminska, Immune microenvironment of gliomas, Lab. Invest. J. Tech. Methods Pathol. 97 (2017) 498–518.

[8] R.R. Weichselbaum, H. Liang, L. Deng, Y.X. Fu, Radiotherapy and immunotherapy: a beneficial liaison? Nat. Rev. Clin. Oncol. 14 (2017) 365–379.

[9] P. John, Y. Wei, W. Liu, M. Du, F. Guan, X. Zang, The B7x immune checkpoint pathway: from discovery to clinical trial, Trends Pharmacol. Sci. 40 (2019) 883–896.

[10] G. Chen, A.C. Huang, W. Zhang, G. Zhang, M. Wu, W. Xu, et al., Exosomal PD-L1 contributes to immunosuppression and is associated with anti-PD-1 response, Nature 560 (2018) 382–386.

[11] G. van Niel, G. D'Angelo, G. Raposo, Shedding light on the cell biology of extracellular vesicles, Nat. Rev. Mol. Cell Biol. 19 (2018) 213–228.

[12] J. Gourlay, A.P. Morokoff, R.B. Luwor, H.J. Zhu, A.H. Kaye, S.S. Stylli, The emergent role of exosomes in glioma, J. Clin. Neurosci. : Off. J. Neurosurg. Soc. Australasia 35 (2017) 13–23.

[13] R. Lane, T. Simon, M. Vintu, B. Solkin, B. Koch, N. Stewart, et al., Cell-derived extracellular vesicles can be used as a biomarker reservoir for glioblastoma tumor subtyping, Commun. Biol. 2 (2019) 315.

[14] M.F. Baietti, Z. Zhang, E. Mortier, A. Melchior, G. Degeest, A. Geeraerts, et al., Syndecan-syntenin-ALIX regulates the biogenesis of exosomes, Nat. Cell Biol. 14 (2012) 677–685.

[15] B.K. Choi, K. Fujiwara, T. Dayaram, Y. Darlington, J. Dickerson, M.A. Goodell, et al., WIP1 dephosphorylation of p27(Kip1) Serine 140 destabilizes p27(Kip1) and reverses anti-proliferative effects of ATM phosphorylation, Cell Cycle 19 (2020) 479–491.

[16] K.T. Chan, S. Blake, H. Zhu, J. Kang, A.S. Trigos, P.B. Madhamshettiwar, et al., A functional genetic screen defines the AKT-induced senescence signaling network, Cell Death Differ. 27 (2020) 725–741.

[17] S.V. Vasaikar, P. Straub, J. Wang, B. Zhang, LinkedOmics: analyzing multi-omics data within and across 32 cancer types, Nucleic Acids Res. 46 (2018). D956-d63.

[18] R. Kalluri, V.S. LeBleu, The biology, function, and biomedical applications of exosomes, Science 367 (2020) 1–15.

[19] A.N. Blackford, S.P. Jackson, ATM, ATR, and DNA-PK: the trinity at the heart of the DNA damage response, Mol. Cell 66 (2017) 801–817.

[20] Y. Yao, H. Ye, Z. Qi, L. Mo, Q. Yue, A. Baral, et al., B7-H4(B7x)-Mediated cross-talk between glioma-initiating cells and macrophages via the IL6/JAK/STAT3 pathway lead to poor prognosis in glioma patients, Clin. Cancer Res. : Off. J. Am. Assoc. Cancer Res. 22 (2016) 2778–2790.

[21] S. Leung, X. Liu, L. Fang, X. Chen, T. Guo, J. Zhang, The cytokine milieu in the interplay of pathogenic Th1/Th17 cells and regulatory T cells in autoimmune disease, Cell. Mol. Immunol. 7 (2010) 182–189.

[22] Y. Wang, Z.G. Liu, H. Yuan, W. Deng, J. Li, Y. Huang, The Reciprocity between Radiotherapy and Cancer Immunotherapy, vol. 25, 2019, pp. 1709–1717.

[23] Y. Muroyama, T.R. Nirschl, C.M. Kochel, Z. Lopez-Bujanda, D. Theodros, W. Mao, et al., Stereotactic radiotherapy increases functionally suppressive regulatory T cells in the tumor microenvironment, Canc. Immunol. Res. 5 (2017) 992–1004.

[24] A.B. Sharabi, C.J. Nirschl, C.M. Kochel, T.R. Nirschl, B.J. Francica, E. Velarde, et al., Stereotactic radiation therapy augments antigen-specific PD-1-mediated antitumor immune responses via cross-presentation of tumor antigen, Canc. Immunol. Res. 3 (2015) 345–355.

[25] M.N. Theodoraki, S.S. Yerneni, T.K. Hoffmann, W.E. Gooding, T.L. Whiteside, Clinical significance of PD-L1(+) exosomes in plasma of head and neck cancer patients, Clin. Cancer Res. : Off. J. Am. Assoc. Cancer Res. 24 (2018) 896–905.

[26] F.L. Ricklefs, Q. Alayo, H. Krenzlin, A.B. Mahmoud, M.C. Speranza, H. Nakashima, et al., Immune evasion mediated by PD-L1 on glioblastoma-derived extracellular vesicles, Sci. Adv. 4 (2018) eaar2766.

[27] H.L. MacGregor, P.S. Ohashi, Molecular pathways: evaluating the potential for B7-H4 as an immunoregulatory target, Clin. Cancer Res. : Off. J. Am. Assoc. Cancer Res. 23 (2017) 2934–2941.

[28] J.R. Podojil, S.D. Miller, Potential targeting of B7-H4 for the treatment of cancer, Immunol. Rev. 276 (2017) 40–51.

[29] R. Wu, J. Zeng, J. Yuan, X. Deng, Y. Huang, L. Chen, et al., MicroRNA-210 overexpression promotes psoriasis-like inflammation by inducing Th1 and Th17 cell differentiation, J. Clin. Invest. 128 (2018) 2551–2568.

[30] R. M, K. M, Z. M, H. J, L. P, O. J, et al., Transcription factor p73 regulates Th1 differentiation, Nat. Commun. 11 (2020) 1475.

[31] H. Sato, A. Niimi, T. Yasuhara, T.B.M. Permata, Y. Hagiwara, M. Isono, et al., DNA double-strand break repair pathway regulates PD-L1 expression in cancer cells, Nat. Commun. 8 (2017) 1751.

[32] D. Han, T. Yu, N. Dong, B. Wang, F. Sun, D. Jiang, Napabucasin, a novel STAT3 inhibitor suppresses proliferation, invasion and stemness of glioblastoma cells, J. Exp. Clin. Cancer Res. : CR (Clim. Res.) 38 (2019) 289.